GROUND EFFECT MODELING FOR ROTARY-WING SIMULATION

Vladimir Khromov and Omri Rand
Technion – Israel Institute of Technology, Israel

Keywords: *rotary-wing, ground effect, flight simulation*

Abstract

The regimes of climb and descent with forward flight are important ingredients in the operation scenarios of both full-scale helicopters and small-scale rotary-wing vehicles as ground effect has a considerable influence on rotor performance.

Within real-time simulations, when even trivial iterative process should be avoided, it is desired to have an explicit (i.e. non-iterative) expression for the induced velocity for all flight regimes, in or out ground effect (IGE, OGE).

The current study presents a rotor wake modeling for the rotor inflow analysis in combined forward and axial flight for both IGE and OGE cases. The methodology is based on the modeling of the upwash induced by the ground at the rotor disk level. The results presented in this paper allow the implementation of the ground effect during real-time simulation.

Nomenclature

C_T Rotor thrust coefficient
C_Q Rotor torque coefficient
P Rotor shaft power
R Rotor disk radius
T Rotor thrust, positive upwards
U_F Free stream velocity
$\bar{V}_a$ Normal-to-disk component of free stream velocity, normalized by v_h, positive downwards (for forward flight $\bar{V}_a = (U_F/v_h)\sin\alpha_D$)
$\Delta\bar{V}_a$ Normal-to-disk component of the ground-reflected stream velocity, normalized by v_h, positive downwards
$\bar{v}$ Rotor mean induced velocity normalized by v_h, positive downwards
$\bar{v}_a$ Rotor mean induced velocity in axial flight, normalized by v_h, positive downwards
v_h Rotor mean induced velocity in hover, positive downwards $\left(=\Omega R\sqrt{C_T/2}\right)$
α Angle of attack
α_D Disk angle
θ Pitch angle
$\bar{\lambda}$ Rotor inflow ratio normalized by v_h, positive downwards
μ Advance ratio $\left(=(U_F/\Omega R)\cos\alpha_D\right)$
$\bar{\mu}$ Advance ratio normalized by $v_h/\Omega R$ (i.e., $=(U_F/v_h)\cos\alpha_D = \mu\sqrt{2/C_T}$)
ρ Air density
σ Rotor solidity
χ Wake skew angle
Ω Rotor angular velocity

Subscripts
a axial
h hover
tip blade tip
co blade cutout

1 Generalization of Existing Experimental Data

One of the ways to analyze a helicopter rotor in the ground proximity is to study the ground reflected upwash and its effect on the rotor performance. The "ground effect" phenomenon may be directly measured as a reduction in the

required (induced) power for a given thrust level, or as an increase in the rotor thrust for a given (induced) power level. In [1]-[6] different approaches to analyze this phenomenon are described and discussed. The global influence of the ground may be quantified for constant induced power as $T_{IGE}/T_{OGE}\big|_{P=const} = k_G(\bar{z})$ or, for constant thrust as $P_{IGE}/P_{OGE}\big|_{T=const} = 1/k_G(\bar{z})$, where $\bar{z} = z/R$ is "ground-rotor" clearance. Hence, it is clear that for constant induced power

$$\bar{\lambda}_{OGE} = k_G \bar{\lambda}_{IGE} \quad . \tag{1.1}$$

Cheeseman & Bennett [1] carried out ground effect analysis from which the following expression has been obtained

$$\frac{T_{IGE}}{T_{OGE}} = k_G = \frac{1}{1-\frac{1}{16}\left(\frac{R}{z}\right)^2\left[\frac{1}{1+(V/v)^2}\right]} \tag{1.2}$$

where, V is the airspeed velocity and v is the inflow induced by the rotor normal to the disk. Alternatively, with the incorporation of the influence of the blade loading

$$k_G = 1+\frac{\rho a N_b c R^3 \Omega^2}{4T_{OGE}}\frac{\lambda}{16\left(\frac{z}{R}\right)^2\left[1+\left(\frac{V}{v}\right)^2\right]} \tag{1.3}$$

where, $\lambda = \eta\lambda_h$, and η is a non-dimensional parameter depending on the forward speed.

Hayden [2] formulated the ground effect for a hovering rotor as

$$C_P = C_{P_0} + k_G^{-1}\left(C_{P_i}\right)_\infty \tag{1.4}$$

where $k_G = 0.9926 + 0.03794(2R/z)^2$.

For hovering rotor, Johnson [3] presents a sketch of thrust increase at constant power for low and high blades loading. Fig. 1 presents increasing in hovering rotor thrust versus ground-rotor distance for the above described expressions.

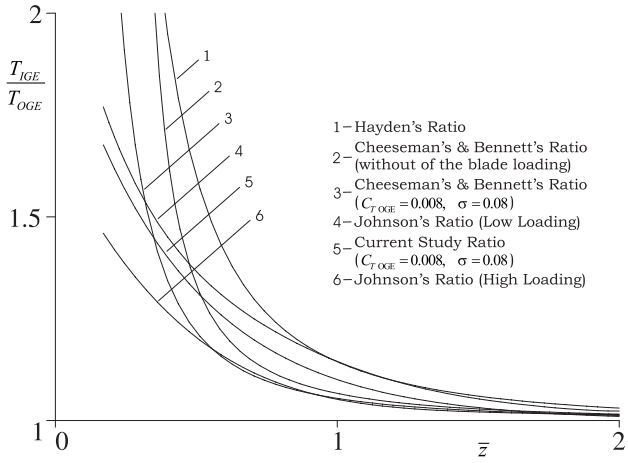

Fig. 1. Influence the Ground Proximity on Rotor Thrust in Hover.

Cheesemann and Bennett [1] indicated that theoretical prediction agrees fairly well with flight tests results at all forward flight regimes only for values of z/R greater than 0.6. The explanation for this fact is the dramatically (non-physical) rise of thrust for smaller ground-rotor distances. Similar behavior of thrust ratio is observed in Hayden's correlation as well. Reference [3] sketch shows more moderate increasing of rotor thrust near the ground for distances of less than half of a rotor radius.

Reference [3] thrust ratio may be approximated by following expressions

$$\frac{T_{IGE}}{T_{OGE}} = k_G \approx 1 + e^{-2\bar{z}} \quad (\text{low loading}) \tag{1.5}$$

and

$$\frac{T_{IGE}}{T_{OGE}} = k_G \approx 1 + e^{-2\sqrt{2}\bar{z}} \quad (\text{high loading}). \tag{1.6}$$

According to [7], the induced ratio in forward flight may be presented in the current terms as $\lambda = \lambda_h/\sqrt{1+\bar{\mu}^2}$. Correspondently, the modified expression (1.3) may be written as

$$\frac{T_{IGE}}{T_{OGE}} = 1+\frac{1}{4}\frac{a\sigma}{C_{T_{OGE}}}\frac{\lambda_h}{16\left(\frac{z}{R}\right)^2\left(1+\bar{\mu}^2\right)^{3/2}} = \tag{1.7}$$

$$= 1+\frac{1}{8G\cdot\bar{z}^2}\left(1+\bar{\mu}^2\right)^{-3/2},$$

where

$$G=\frac{8C_{T_{OGE}}}{a\sigma\lambda_h}\approx\frac{2\sqrt{C_{T_{OGE}}}}{\sigma}. \qquad (1.8)$$

Based on (1.5), (1.6), and (1.8), a generalized function of the thrust ratio versus ground-rotor distance may be expressed as

$$\frac{T_{IGE}}{T_{OGE}}=1+e^{-G\cdot\bar{z}}\left(1+\bar{\mu}^2\right)^{-3/2}, \qquad (1.9)$$

see Fig. 1 also.

Note that the above expression for k_G reaches the value of 2 in hover for $\bar{z}=0$ and not infinity as shown in some of the above references. This characteristic will be shown to be important in what follows.

2 Ground Effect Modeling

2.1 The Upwash Reflected from the Ground

The OGE induced velocity in axial flight normalized by v_h, $\bar{v}\left(\bar{V}_a\right)$, may be expressed by three piecewise functions from axial velocity $\left(\bar{V}_a\right)$ for climb, low descent and high descent. Climb and high descent equations are the exact momentum theory expressions respectively. The low descent equation represents a rational curve-fitting of experimental results. This curve-fitting satisfies continuity of value and derivative for $\bar{V}_a=0$ and $\bar{V}_a=-2$. Ref. [7] proposed to look at the induced velocity in forward flight as the product of the induced velocity, $\bar{v}_a$, which would has been generated in axial flight for the actual normal ("climb/descent") velocity $\left(\bar{V}_a\right)$, and a decay factor of $1/\sqrt{1+\bar{\mu}^2}$ which is caused by the in-plane velocity component $\left(\bar{\mu}\right)$. It was therefore, proposed to replace Glauert's equation by the following estimation of the induced inflow:

$$\bar{v}=\frac{\bar{v}_a}{\sqrt{1+\bar{\mu}^2}}=\frac{1}{\sqrt{1+\bar{\mu}^2}}\times$$
$$\times\begin{cases}-\frac{1}{2}\bar{V}_a+\sqrt{\frac{\bar{V}_a^{\,2}}{4}+1}, & \bar{V}_a\geq 0\\ 1-\frac{1}{2}\bar{V}_a+\frac{7}{8}\bar{V}_a^{\,2}+\frac{9}{16}\bar{V}_a^{\,3}, & -2<\bar{V}_a<0\\ -\frac{1}{2}\bar{V}_a-\sqrt{\frac{\bar{V}_a^{\,2}}{4}-1}, & \bar{V}_a\leq -2\end{cases} \qquad (2.1)$$

The axial rotor inflow far from ground consists of two components: the rotor induced velocity $\left(\bar{v}=\bar{v}\left(\bar{\mu},\bar{V}_a\right)\right)$ and normal-to-the disk component of the free stream velocity $\left(\bar{V}_a=\bar{V}_a\left(\alpha_D\right)\right)$. The direction of last component defines the rotor axial flight regime – "climbing" $\left(\bar{V}_a>0\right)$, "hovering" $\left(\bar{V}_a=0\right)$ or "descending" $\left(\bar{V}_a<0\right)$. Near the ground the axial rotor inflow includes an additional component: the normal-to-disk component of the ground-reflected upwash $\left(\Delta\bar{V}_a<0\right)$. Hence, for IGE rotor the sum $\bar{V}_A=\left(\bar{V}_a+\Delta\bar{V}_a\right)$ defines the rotor axial flight regime – climb/hover/descent. At this stage, one can examine two cases:

Case I: $\bar{V}_a\geq 0$ - i.e., forward flight with climbing. In this case the OGE rotor inflow ratio may be written as

$$\bar{\lambda}_{OGE}^{C}=\frac{1}{\sqrt{1+\bar{\mu}^2}}\left(-\frac{1}{2}\bar{V}_a+\sqrt{\frac{\bar{V}_a^{\,2}}{4}+1}\right)+\bar{V}_a \qquad (2.2)$$

and the corresponding inflow ratio IGE may be expressed for $\bar{V}_A\geq 0$ as

$$\bar{\lambda}_{IGE}^{C}=\frac{1}{\sqrt{1+\bar{\mu}^2}}\left[-\frac{1}{2}\bar{V}_A+\sqrt{\frac{\bar{V}_A^{\,2}}{4}+1}\right]+\bar{V}_A, \qquad (2.3)$$

and for $\bar{V}_A<0$, as

$$\bar{\lambda}_{IGE}^{D} = \frac{1}{\sqrt{1+\bar{\mu}^2}} \times \times \left[1 - \frac{1}{2}\bar{V}_A + \frac{7}{8}\bar{V}_A{}^2 + \frac{9}{16}\bar{V}_A{}^3\right] + \bar{V}_A . \quad (2.4)$$

Case II: $\bar{V}_a < 0$ - i.e., forward flight with descending. The OGE rotor inflow ratio may be expressed as

$$\bar{\lambda}_{OGE}^{D} = \frac{1}{\sqrt{1+\bar{\mu}^2}} \times \times \left(1 - \frac{1}{2}\bar{V}_a + \frac{7}{8}\bar{V}_a{}^2 + \frac{9}{16}\bar{V}_a{}^3\right) + \bar{V}_a . \quad (2.5)$$

and the corresponding IGE inflow ratio is expressed by Eq. (2.4) - in this case $\bar{V}_A < 0$. Note that the high descent regime is not applicable for ground effect as will be shown later on.

Hence, the constant power equations (1.1) may be presented for "OGE climb - IGE climb", "OGE climb - IGE descent", and "OGE descent - IGE descent" flight modes as

$$\begin{aligned} &\bar{\lambda}_{OGE}^{C} = k_G \bar{\lambda}_{IGE}^{C}, \ for \ \bar{V}_a \geq 0 \ and \ \bar{V}_A \geq 0 \\ &\bar{\lambda}_{OGE}^{C} = k_G \bar{\lambda}_{IGE}^{D}, \ for \ \bar{V}_a \geq 0 \ and \ \bar{V}_A < 0 \\ &\bar{\lambda}_{OGE}^{D} = k_G \bar{\lambda}_{IGE}^{D}, for \ \bar{V}_a < 0. \end{aligned} \quad (2.6)$$

The first equation of Eq. (2.6) illustrates the normal working state for climbing rotor near the ground where the ground-reflected upwash is smaller than or equal to the climb velocity, which gives an "equivalent slower climb" $\left(\bar{V}_A = \bar{V}_a + \Delta\bar{V}_a\right) > 0$. The second and third equations of Eq. (2.6) describe an "equivalent vortex-ring state", i.e $\left(\bar{V}_A = \bar{V}_a + \Delta\bar{V}_a\right) < 0$. The upper boundary of this state is the "equivalent hover" while the lower boundary of it is the state where the rate of descent is equal to the average induced velocity, i.e. where the net flow through the disk vanishes $\left(\bar{V}_a + \bar{v} = 0 \text{ and } \Delta\bar{V}_a = 0\right)$ which will be denoted in what follows as an "equivalent parachute state".

For large rates of descent, the net flow through the disk is directed upwards which rules out any ground effect.

The above discussion for rotor in axial flight is demonstrated in Fig. 2. This figure presents the real solution of Eqs. (2.6) based on the generalized function for the thrust ratio (1.9).

The ground influence leads to increasing of induced velocity since the rotor is working in an equivalent descent regime. However, the sum of the induced, the (dynamic) axial and the ground-reflected velocities is decreasing. As shown, the above theoretical curves coincide with the OGE momentum theory for axial flight regimes since by increasing the ground-rotor distance, the IGE curves transfigure to OGE flight mode. It also supports the discussion in [3], where the ground effect is generally negligible when the hovering rotor is more than one diameter above the ground.

As shown, the curves for all ground-rotor distances converge into the equivalent parachute state point where no net flow through the rotor is produced.

Fig. 3 presents the real solution of Eq. (2.6) for forward flight with climbing/descending near the ground based on the generalized function for the thrust ratio (1.9). As shown, the above discussion for rotor at axial flight regimes near the ground is still valid (decrease of the ground influence with increase of ground-rotor distance and crossing in "Parachute State" point). In addition, the ground effect decreases with the increase of forward flight velocity, and vanishes for $\bar{\mu} > 2$. It also coincides with discussion in [3].

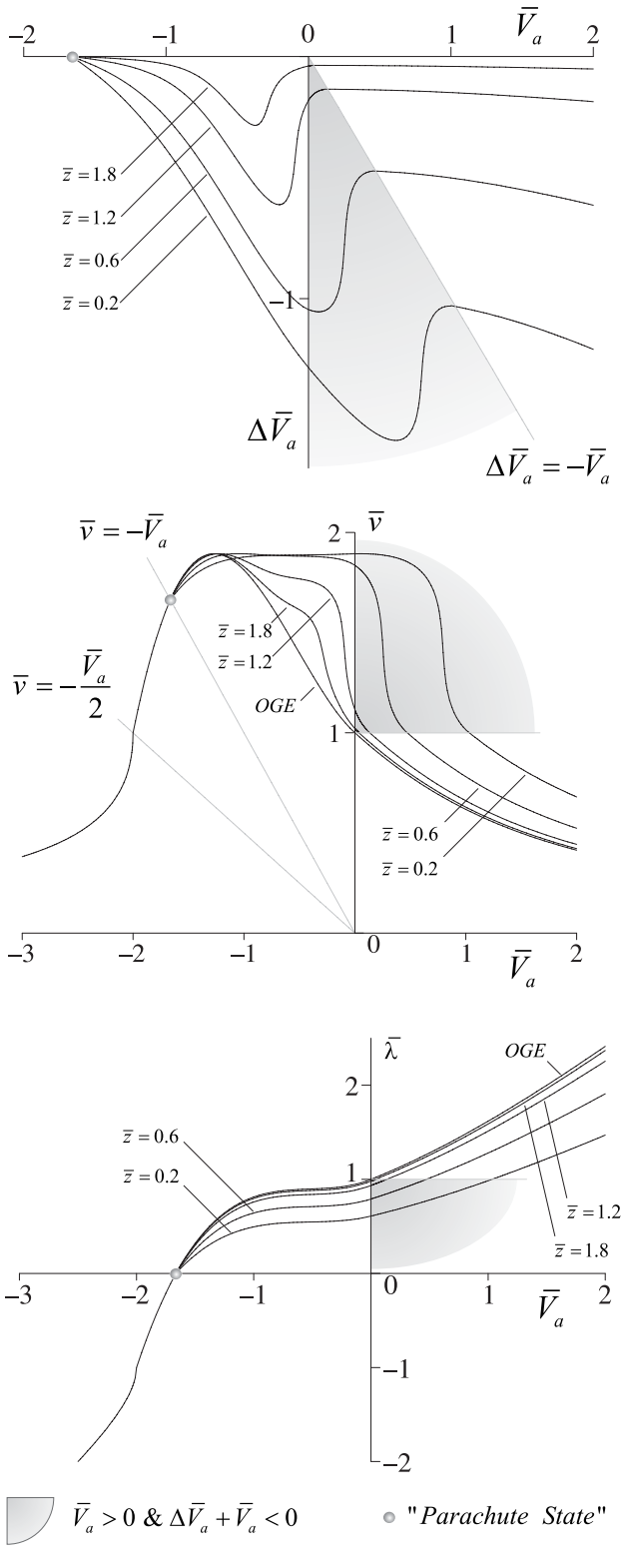

Fig. 2. Reflected, Induced Velocity and Rotor Inflow in Climb/Hover/Descent $(\bar{\mu}=0,\ C_{T\ OGE}=0.008,\ \sigma=0.08)$

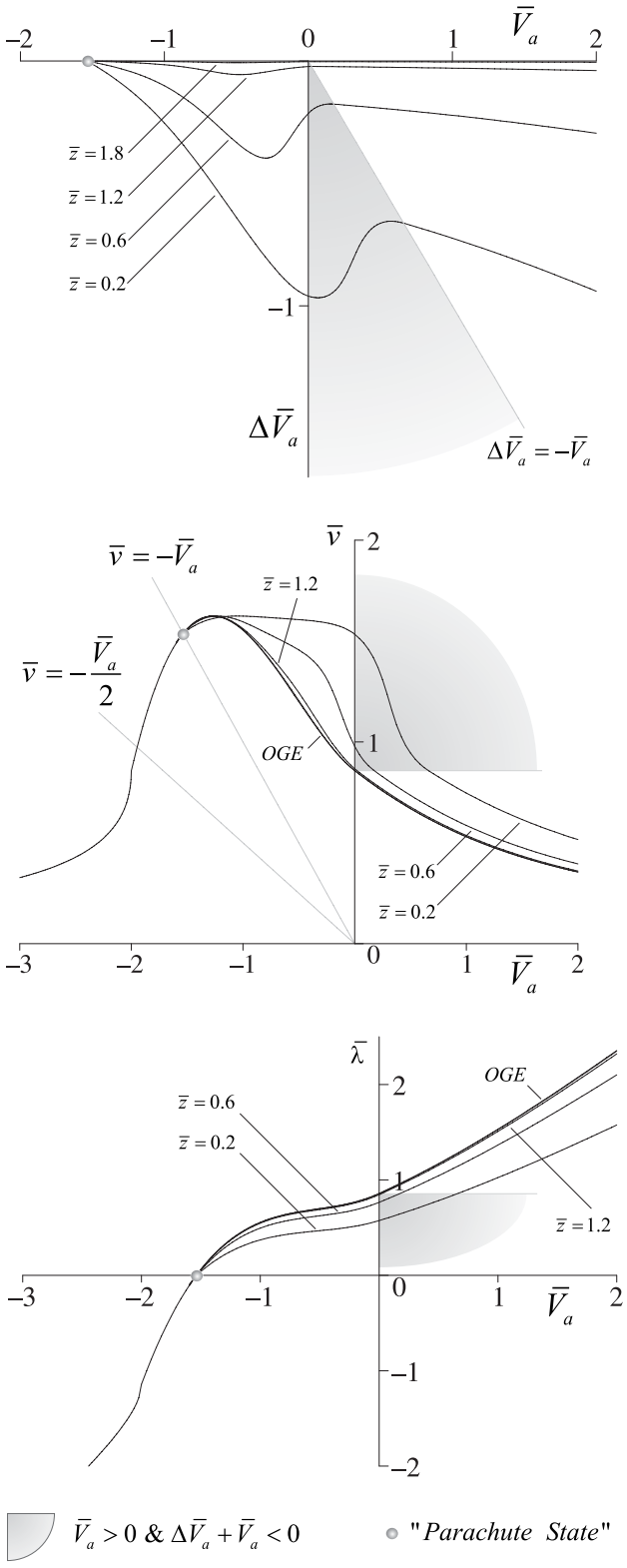

Fig. 3. Reflected, Induced Velocity and Rotor Inflow in Forward Flight with Climbing/Descending $(\bar{\mu}=0.6,\ C_{T\ OGE}=0.008,\ \sigma=0.08)$

2.2 The Ground Effect Influence on the Rotor Wake

The above analysis allows some insight into the forward flight rotor wake approximate geometry and the flight velocity. The IGE rotor wake skew angle (χ) is defined by the forward flight velocity and inflow as $\chi = \tan^{-1}\left(\bar{\mu}/\bar{\lambda}_{IGE}\right)$ - see Fig. 4.

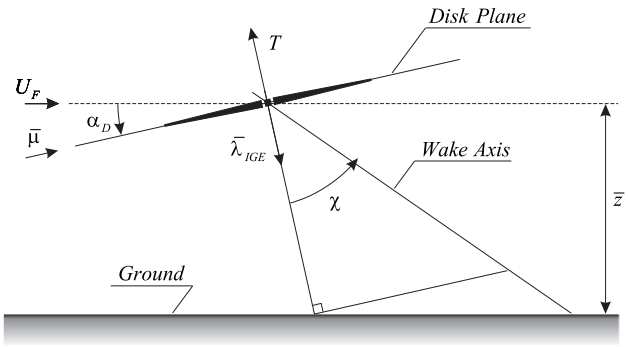

Fig. 4. IGE Rotor Wake Slope Notation

Fig. 5 and Fig. 6 present the information included in thrust ratio approximations (Eqs. (1.7), (1.9)) and the relations between inflow ratios, rotor height, flight velocity and the skew angle.

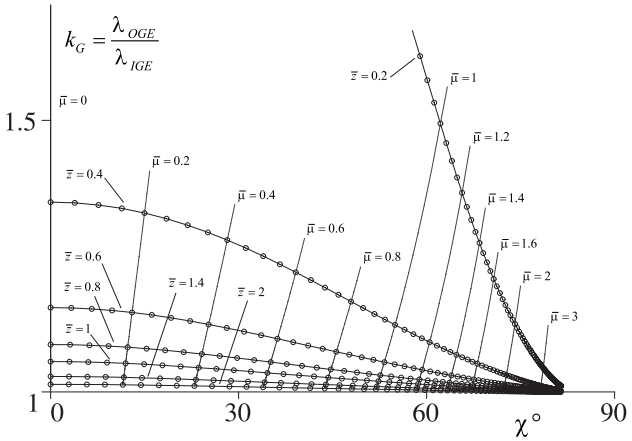

Fig. 5. Wake Skew Angle of Rotor Near the Ground - Cheesemann and Bennett research [1] $\left(C_{T\ OGE} = 0.008,\ \sigma = 0.08,\ \alpha_D = 7°\right)$

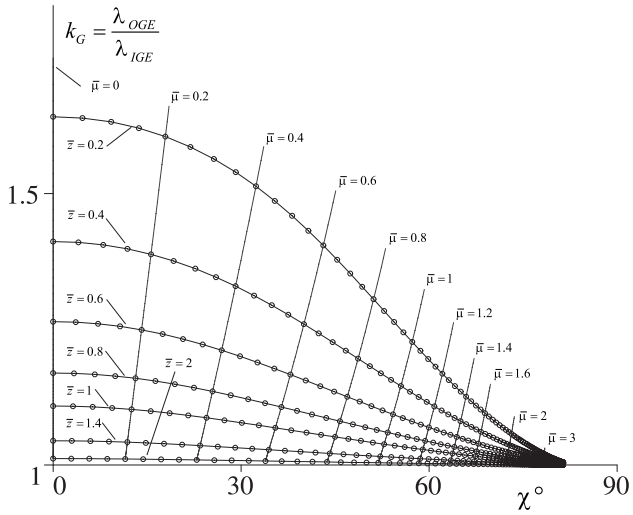

Fig. 6. Wake Skew Angle of Rotor Near the Ground – Current Study $\left(C_{T\ OGE} = 0.008,\ \sigma = 0.08,\ \alpha_D = 7°\right)$

As shown, the ground effect influence on the wake skew angle is negligible for ground-rotor distance above one diameter and speed $\bar{\mu} > 2$. The wake skew angle behavior based on [1] and the current study results for ground-rotor distances above 0.6 rotor radius is similar for different advance ratios. For smaller distances the skew angle magnitude based on approximation [1] dramatically increases, and are not applicable as also indicated in [1].

The Fig. 5 and Fig. 6 also correlate with the study reported in [8]. This study shows that when the rotor is in forward flight at a distance more than one-half radius above the ground, the favorable ground effect is essentially vanishes by the time the skew angle has risen to the order of 70º.

2.3 Comparison of the Ground Reflected Velocity and the Change in Inflow at the Rotor Disk

In the current study, the IGE rotor inflow may be expressed as $\bar{\lambda}_{IGE}\left(\bar{V}_A\right) = \bar{v}\left(\bar{V}_A\right) + \bar{V}_A$, where $\bar{V}_A = \bar{V}_a + \Delta\bar{V}_a$. Typically, for IGE rotor performance analysis, a correction for the induced velocity over the rotor disk is written as $\left(\bar{\lambda}_{OGE} + \Delta\bar{\lambda}\right)$ which in the current formulation is equivalent to $\bar{\lambda}_{IGE}\left(\bar{V}_A\right)$, namely

$$\bar{\lambda}_{OGE} + \Delta\bar{\lambda} = \bar{\lambda}_{IGE}\left(\bar{V}_A\right) \qquad (2.7)$$

Hence,

$$\Delta\bar{\lambda} = \begin{cases} \bar{\lambda}^{C}_{IGE} - \bar{\lambda}^{C}_{OGE}, & for \quad \bar{V}_a \geq 0 \quad and \quad \bar{V}_A \geq 0 \\ \bar{\lambda}^{D}_{IGE} - \bar{\lambda}^{C}_{OGE}, & for \quad \bar{V}_a \geq 0 \quad and \quad \bar{V}_A < 0 \\ \bar{\lambda}^{D}_{IGE} - \bar{\lambda}^{D}_{OGE}, & for \quad \bar{V}_a < 0 \end{cases} \quad (2.8)$$

where $\bar{\lambda}^{C}_{OGE}$, $\bar{\lambda}^{D}_{OGE}$, $\bar{\lambda}^{C}_{IGE}$, and $\bar{\lambda}^{D}_{IGE}$ are defined by Eqs. (2.2) - (2.5).

Comparison between $\Delta\bar{\lambda}$ and $\Delta\bar{V}_a$ is presented in Fig. 7.

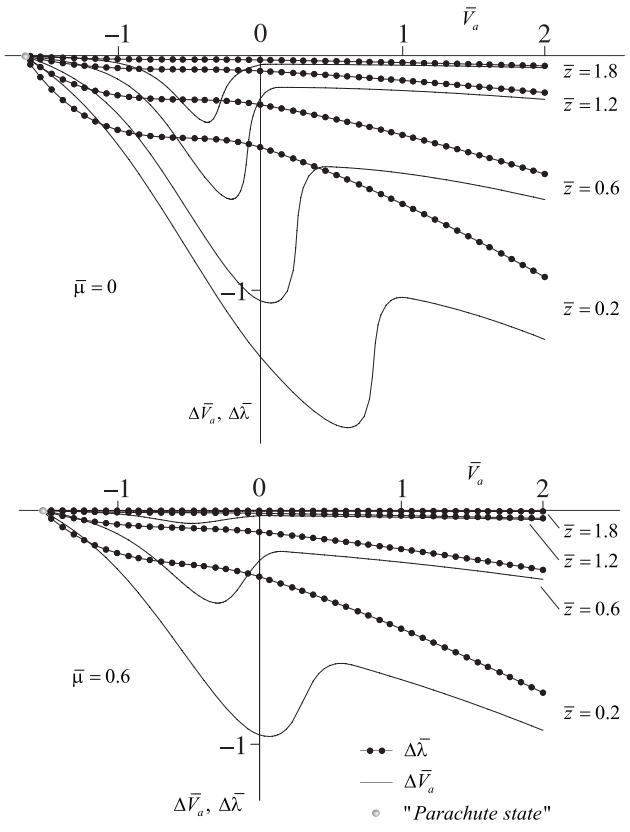

Fig. 7. $\Delta\bar{V}_a$ and $\Delta\bar{\lambda}$ vs. Axial Velocity $\left(C_{T\,OGE} = 0.008,\ \sigma = 0.08\right)$

As shown, the magnitudes and behavior of $\Delta\bar{\lambda}$ and $\Delta\bar{V}_a$ are significantly different which means that in the classical approach, $\Delta\bar{\lambda}$ is not the ground-reflected upwash.

Note that the variations of the ground-reflected velocity with respect to $\Delta\bar{V}_a$ are compensating by the variations in the induced velocity (see Fig. 2, Fig. 3).

3 Correlation and Validation

3.1 Correlation with Hovering Rotor Experimental Data

To correlate the above generalized methodology with experimental results, a generic "Momentum-Blade-Element" analysis with uniform inflow has been employed. The analysis scheme is capable of incorporating non-uniform blades and incorporates calibrated by OGE test data nonlinear two-dimensional airfoil characteristics by using look-up technique for the aerodynamic tables that simulate stall, Mach and Reynolds number effects. The tabular values of the lift, the drag and the aerodynamic moment coefficients are approximated by as three-dimensional piecewise polynomials, namely:

$$\begin{aligned} c_l &= f_{cl}\left(\alpha(r), M(r), \mathrm{Re}(r)\right) \\ c_d &= f_{cd}\left(\alpha(r), M(r), \mathrm{Re}(r)\right) \\ c_m &= f_{cm}\left(\alpha(r), M(r), \mathrm{Re}(r)\right) \end{aligned} \quad (3.1)$$

The thrust and torque expressions for IGE rotor may be put in a general form as:

$$\begin{aligned} C_T &= \int_{R_{co}}^{R_{tip}} f_{C_T}\left(\bar{\lambda}_{IGE}\left(\bar{V}_A\right),\ \theta_0,\ c_l\right) dr \\ C_Q &= \int_{R_{co}}^{R_{tip}} f_{C_Q}\left(\bar{\lambda}_{IGE}\left(\bar{V}_A\right),\ \theta_0,\ c_d\right) dr \end{aligned} \quad (3.2)$$

where

$$\alpha = \theta_0 + \alpha_{twist}(r) - \frac{\bar{\lambda}_{IGE}\left(\bar{V}_A\right) v_h}{r/R} \quad (3.3)$$

The experimental results were produced by the rotor-ground setup of a closed 21×23×16-foot laboratory at Ames Research Center. The rotor blades were fashioned after a full-scale version of the XV-15 rotor and the blades section are based on the NACA 64 series. The detailed test description of the experiments and test conditions was presented in [9].

Fig. 8 presents the correlation between the C_T/σ, C_Q/σ and Figure of Merit (FOM) obtained in the experiment and the predicted values vs. the normalized ground distance

$\bar{z} = z/R$ for constant pitch angle of $\theta_{0.75} = 10.87°$.

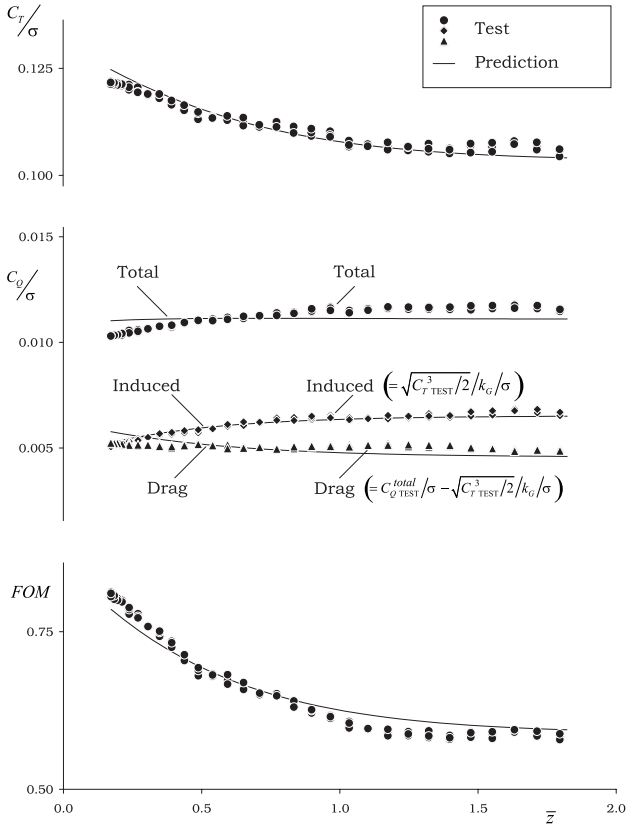

Fig. 8. Thrust, Torque & FOM vs. $\bar{z}$ for $\theta_{0.75} = 10.87°$

The above correlation has been executed by taking the pitch angle and the "ground-rotor" distance as given data and employ the above described semi-analytic methodology to predict the required thrust, and the power values. First, it is shown that the correlation of the thrust and the total required power are reasonable. In addition, the model shows that while the total power is only slightly decreasing as the rotor-ground distance is reduced, the induced power reduction is much more pronounced. This fact explains the minor increasing of thrust (only 15%) shown in Fig. 8. Thus, this is a classical "intermediate" case of ground effect, where thrust in increasing and power is decreasing which is clearly different from the pure basic empirical law described in Eq. (1.9) that described the case of constant induced power or constant thrust.

Further explanation may be supplied by writing $C_T^{IGE} = f_T C_T^{OGE}$ and $C_P^{IGE} = f_P C_P^{OGE}$. As shown in Fig. 9, the present experiment and prediction were executed for a constant pitch angle that produces $f_T \cong 1.15$ and $f_P \cong 0.76$. "Classical" ground effect (i.e. constant induced power or constant thrust) may be obtained by suitable variation of pitch angle.

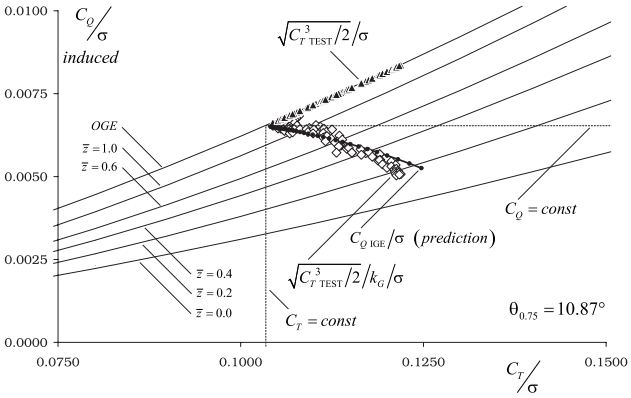

Fig. 9. Torque vs. Thrust for Different Ground-Rotor Distances

Reference [6] discusses the rotor induced velocity reducing nears the ground as the key to the ground effect analysis. It also presents the results of the tests data which were gathering from Knight and Hefner (1941), Bellinger (1972), and Hayden (1976) model and full-scale flight experiments. The induced velocity decreasing is expressed as ratio induced velocity at the rotor in and out of ground effect for constant thrust. Obviously, it is expressed in current term as

$$\frac{\bar{\lambda}_{IGE}(\bar{z})}{\bar{\lambda}_{OGE}} = \\ = k_G\left(1 + \frac{1}{2}\Delta\bar{V}_a + \frac{7}{8}\Delta\bar{V}_a^{\,2} + \frac{9}{16}\Delta\bar{V}_a^{\,3}\right) \qquad (3.4)$$

Fig. 10 presents the results of the analytical study in comparison with above tests data.

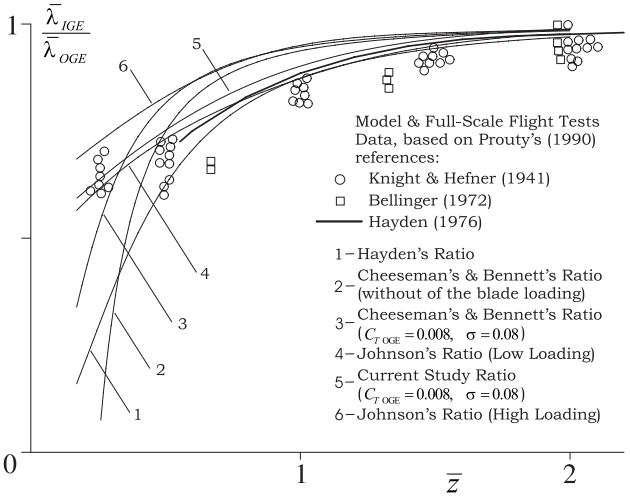

Fig. 10. Hovering Rotor Induced Velocity Ratio vs. $\bar{z}$

3.2 Illustrative Results for Rotor in Forward Flight

Illustrative examples for IGE rotor in forward flight are presented in Fig. 11- Fig. 12.

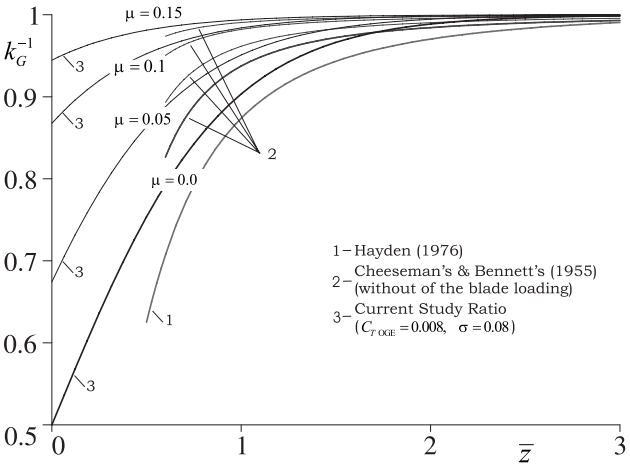

Fig. 11. Ground Effect on Rotor Induced Power vs. Ground-Rotor Distance for Several Forward Flight Velocities

Fig. 11 presents the ground influence on the rotor induced power. Eq. (1.1) describes the induced power ratio near and far from the ground for constant thrust. The current analytical results for OGE and IGE forward flight rotor are presented in comparison with Cheeseman & Bennett [1] approximation for forward flight and Hayden [2] approximation for hover.

As shown, the current results for hover are between the above approximations. The current results for IGE forward flight rotor are closed to those of [1] for ground-rotor distances (z/R) of more than 0.6. In addition, the ground influence on the rotor vanishes for $\mu > 0.15$ (see [3] also).

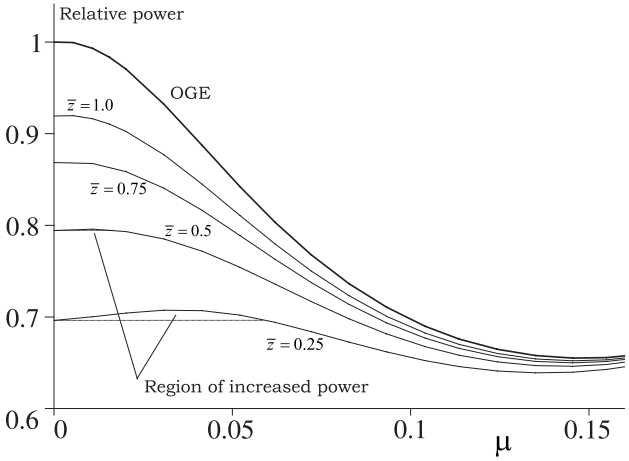

Fig. 12. Example of Ground Effect on Rotor Total Power vs. Forward Flight Velocity for Several Ground-Rotor Distances $\left(C_{T\,OGE}=0.008,\ \sigma=0.08,\ \alpha_D=4^\circ,\ 800RPM\right)$

Fig. 12 presents analytical study of the ground effect on the total power vs. forward flight velocity for several ground-rotor distances. The ground influence is limited by ground-rotor distance $z/R<2$ and velocity of $\mu<0.15$. The increasing ground-rotor distance leads to OGE required power. The figure illustrates the increasing power region during transition from hover to forward flight for small ground-rotor distances (see discus in [6]).

4 Implementation of Ground Effect Modeling in Flight Simulation

For an OGE rotor in the forward flight with climbing/descending, the flow through the disk is composed of the total axial velocity (i.e. normal-to-disk component of free stream velocity) plus the corresponding induced velocity. For IGE rotor the flow through the disk includes the total axial vehicle velocity, normal-to-disk component of the ground-reflected upwash velocity at the rotor disk level and the induced velocity (which is also a function of the ground proximity).

Hence, during current integration step the main rotor thrust, advance and inflow ratios,

dynamic axial velocity and flight height values define the magnitude of the upwash induced by the ground. At the next integration step the sum of the dynamic velocity, the rotor induced velocity and the upwash determine the flow through the main rotor disk.

The above presented discussion allows to reproduce the rotor flight dynamics during real-time simulation based on the actually rotor height above the ground.

Scheme of the ground effect model implementation during flight simulation is presented in Fig. 13.

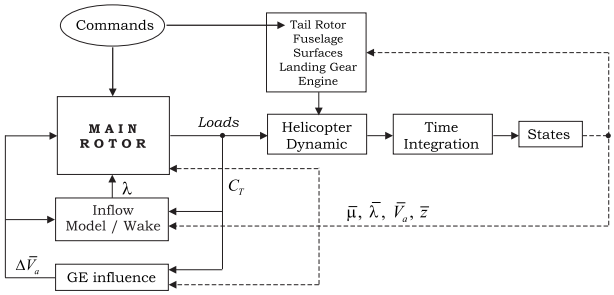

Fig. 13. Ground Effect Modeling Scheme

Conclusions

A method for modeling rotor performances in ground effect for flight simulation is offered. The method is based on the rotor inflow analysis for forward and axial flight modes combinations for both IGE and OGE cases and takes into account the ground-reflected upwash at the rotor disk level. The method allows efficient determination of the rotor flight dynamics during real-time simulation with and without wake model.

References

[1] Cheeseman I, and Bennett W. "The effect of the ground on a helicopter rotor in forward flight", ARC R&M 3021, September 1955.

[2] Hayden J. "The effect of the ground on helicopter hovering power required", *AHS 32nd Forum*, 1976.

[3] Johnson W. *Helicopter theory*. Dover Publications, Inc., 1994.

[4] Leishman J. *Principles of helicopter aerodynamics*. Cambridge University Press, 2001.

[5] Padfield G. *Helicopter flight dynamics: the theory and application of flying qualities and simulation modeling*. AIAA, Inc., 1996.

[6] Prouty R. *Helicopter performance, stability, and control*. Robert E.Krieger Publishing Company, Inc., 1990.

[7] Rand O. "A phenomenological modification for Glauert's classical induced velocity equation", *Journal of American Helicopter Society*, Vol. 51, No. 3, pp. 279 – 282, 2006.

[8] Heyson H. "Ground effect for lifting rotors in forward flight", NASA-TN-D-234, Washington, May 1960.

[9] McAlister K, Tung C, Rand O, Khromov V, and Wilson J. "Experimental and numerical study of a model coaxial rotor", *Additional Proceedings Papers of the American Helicopter Society 62nd Annual Forum*, Phoenix, Arizona, 2006.

Copyright Statement